Subgrid CFD Film-drainage Modelling:
Application to Buoyancy-driven Droplet–wall Collisions in Emulsions

L. R. Mason, G. W. Stevens and D. J. E. Harvie

Department of Chemical and Biomolecular Engineering,
The University of Melbourne, Victoria 3010, Australia

Abstract

The buoyancy-driven interaction between a free droplet and solid wall is simulated. The presented model makes use of the continuum-surface-force (CSF) framework to couple an interface-capturing technique to a lower-dimensional lubrication reduction of the thin-film momentum equation. Droplet-scale fluid transport was modelled using an axisymmetric level-set method, including a reinitialisation procedure. Through comparison of model results with experimental data from the literature, we demonstrate the effectiveness of this approach in simulating the challenging problem of small-length-scale drainage in computational fluid dynamics (CFD) modelling. Film-thickness profiles were modelled up until the onset of asymmetric film-drainage. Results presented will aid in the future improvement of simulation techniques for droplet interactions in liquid–liquid systems.

Introduction

A detailed understanding of droplet–interface and droplet–droplet interactions is required in the design and optimisation of multi-phase industrial processing equipment. Droplet collisions, however, pose unique experimental and numerical challenges due to the large differences in length scales present.

Experimental studies have focused on (i) droplet–wall [5], (ii) droplet–home-phase [2] and (iii) droplet–droplet [4] collision scenarios. Using a capillary, Hartland [6] generated free droplets of known volume that were allowed to fall under buoyancy and collide with a solid surface. Profiles of the film thickness were obtained via tracing magnified photographs of the collision sequence. The refractive indices of the two fluids were matched to minimise optical distortion. A positive pressure was reasoned to exist near the centre of the film in order to drive viscous film drainage, consistent with the observed "dimpling" of the film-thickness profiles. Similar droplet–wall systems have been studied using high-speed video and interferometric techniques [11, 5].

Modelling studies have applied film-thickness based adaptive mesh refinement and moving-mesh interface-tracking methods [14]. To capture the collision dynamics completely, a discretisation mesh is required to span scales from the droplet diameter (typically of order 1–10 mm) to the thickness of the draining film, which can be as low as 10–100 nm prior to the onset of wetting. Alternative approaches have included the coupling of droplet-scale dynamics, via force balances [11] or experimental imaging [12], to semi-analytical thin-film drainage models [3].

In this study, we demonstrate the efficacy of a multi-scale modelling approach that alleviates the need for computationally taxing mesh refinement. A level-set method is coupled to a concurrent numerical solution of the Reynolds lubrication equations using the finite-volume solver *arb* [9]; the coupling is achieved via incorporating the film pressure into the continuum–surface–force (CSF) framework of Brackbill *et al.* [1] A volume-of-fluid based version of the modelling framework has previously been applied to Leidenfrost [10] and binary coalescence [13] dynamics in liquid–gas spray systems. Here, we demonstrate its applicability to droplet–wall collisions in an emulsion system. Direct comparisons are made to the buoyancy-driven collision experiments of Hartland [6].

Numerical Method

Droplet-scale Level-set Model

A level-set method [15] is used to capture multiphase fluid motion: the level-set function, s, is defined via

$$s(\mathbf{x}) = \begin{cases} d(\mathbf{x}), & \text{for } \mathbf{x} \in \text{disperse phase} \\ 0, & \text{on interface} \\ -d(\mathbf{x}), & \text{for } \mathbf{x} \in \text{continuous phase} \end{cases} \quad (1)$$

where $d(\mathbf{x})$ is the minimum normal distance from location $\mathbf{x}$ to the interface. Level-set advection is undertaken using

$$\frac{\partial s}{\partial t} + \nabla \cdot (s\mathbf{u}) = 0, \quad (2)$$

where $\mathbf{u}$ is the fluid velocity. The incompressible Navier–Stokes equations are solved in conservation form:

$$\frac{\partial(\rho\mathbf{u})}{\partial t} + \nabla \cdot (\rho\mathbf{u}\mathbf{u} + p\mathbf{I} + \tau) = \mathbf{f}_b + \rho\mathbf{g} \quad (3)$$

$$\nabla \cdot \mathbf{u} = 0 \quad (4)$$

where the viscous stress tensor, τ, is given by

$$\tau = -\mu\left[\nabla\mathbf{u} + (\nabla\mathbf{u})^\mathsf{T}\right], \quad (5)$$

and $\mathbf{f}_b$ is a CSF source term incorporating the interfacial tension and film pressure forces [1, 10, 13]:

$$\mathbf{f}_b = (\gamma\kappa + p_{\text{film}})\hat{\mathbf{n}} \quad (6)$$

Here, γ, κ and p_{film} are the interfacial tension, local interface curvature and subgrid film pressure, respectively. The volume-averaged volume fraction is then given by $\phi(\mathbf{x}) = H(s(\mathbf{x}))$, where H is a smoothed Heaviside function. The fluid density, ρ, and viscosity, μ, can be related to ϕ via

$$\rho = \phi(\rho_d - \rho_c) + \rho_c \quad (7)$$
$$\mu = \phi(\mu_d - \mu_c) + \mu_c \quad (8)$$

where subscripts "d" and "c" refer to the disperse and continuous phase. Level-set reinitialisation is applied for locations separated further than ε from the interface (figure 1).

Film-scale Lubrication Model

The lubrication equations [10]

$$\frac{\partial p_{\text{film}}}{\partial z} = 0 \quad (9)$$

and

$$\frac{\partial^2 v_r}{\partial z^2} = \frac{1}{\mu_c} \frac{\partial p_{\text{film}}}{\partial r} \qquad (10)$$

are solved on a one-dimensional grid (figure 1a). The radial film velocity, v_r, is subject to a no-slip boundary condition on the solid wall,

$$(v_r)_{z=0} = 0, \qquad (11)$$

and a matched-velocity constraint on the lower droplet interface,

$$(v_r)_{z=h} = (u_r)_{z=h}, \qquad (12)$$

where $h(r)$ is the local film thickness. The local film volumetric flow rate, Q, is determined via

$$Q = 2\pi r h \bar{v}_r, \qquad (13)$$

where $\bar{v}_r$ is the z-averaged local radial velocity from the solution to equation (10). A volume-conservation equation can then be defined on all film cells,

$$A_z \frac{\partial h}{\partial t} = Q_{\text{in}} - Q_{\text{out}}, \qquad (14)$$

where A_z is the annular cell area and Q_{in} and Q_{out} refer to the volumetric flow rates into and out of a cell, respectively, via its faces (figure 1a). We interpolate cell-centred film variables (h, p_{film}) to the film faces using an integral interpolation method based on an analytical solution to equation (10). Reflection boundary conditions are applied on the $r = 0$ centreline, and the film pressure is set to $p_{\text{film}} = 0$ on the outer boundary.

The droplet-scale motion equations, equations (3) and (4), are solved together with the volume-conservation film equation, equation (14), using the finite-volume solver *arb* [9]. Parameter values are given in table 1.

Parameter	0.10 mL	0.25 mL	0.50 mL
D (mm)	5.76	7.82	9.85
z_0/D (–)	0.60	0.60	0.70
$\Delta r/D$ (–)	38	39	36
$\varepsilon/\Delta r$ (–)	1.5	1.5	1.5
ρ_d (kg/m^3)	1.58×10^3	1.58×10^3	1.55×10^3
ρ_c (kg/m^3)	1.07×10^3	1.07×10^3	1.07×10^3
μ_d (Pa s)	17.5	17.5	20.0
μ_c (Pa s)	13.7	13.7	13.7
γ (mN/m)	24.0	24.0	24.2

Table 1. Simulation parameters corresponding to the 0.10, 0.25 and 0.50 mL droplet-volume experimental cases of Hartland [6].

Results and Discussion

Each experimental case of Hartland [6] was investigated, corresponding to droplet volumes, V, of 0.10, 0.25 and 0.50 mL. To highlight the satisfactory agreement between model and experimental results at the small scale of film drainage, time sequences of the film-thickness, $h(r,t)$, and a characteristic film-pressure profile, $p_{\text{film}}(r)$ are given. To demonstrate similarly good agreement at the larger droplet scale, a characteristic cross-sectional droplet profile is presented.

Film-scale Validation

Film-thickness time sequences are shown in figure 2. Simulation results agree well with the corresponding experimental profiles until the onset of asymmetric drainage, which cannot be accounted for using the present axisymmetric model. For each
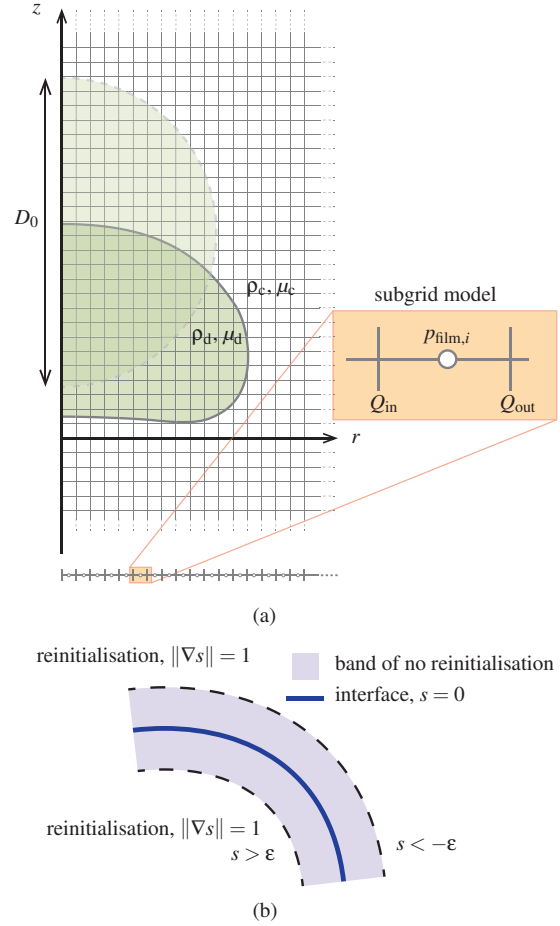
Figure 1. Sketch of modelling approach: (a) droplet-scale domain mesh and subgrid model, (b) level-set reinitialisation scheme.

collision case, the earliest profile presented in [6], at nominal $t = 0$ s, displays flattening consistent with a droplet–wall interaction. As the initial droplet release heights, z_0, are not known from [6], we use an optimised z_0 such that the film thickness deforms to the same extent, at the correct distance from the wall, as the $t = 0$ s experimental profile. Optimum z_0 results are given in table 1 and all simulation times have been translated to be consistent with the quoted experimental times. Simulations of freely accelerating droplets, with no wall present, indicate that the deformation present in the $t = 0$ s experimental profile cannot be attributed to viscous drag. The film-thickness shapes at terminal velocity are shown in figure 2, denoted "terminal profile". Results from additional simulations (not shown) undertaken using perturbed, aspherical droplets of equivalent volume indicated that evolution of the film profile is not highly sensitive to the initial droplet shape, consistent with the numerical results of [8].

Time series for the centreline, h_0, and barrier rim, h_f, film thickness are shown in figure 3 for the 0.1 mL case. The present model agrees well with experimental results for both the centreline and rim thicknesses; note that the model of [8] underestimates the rim thickness at early times in the sequence.

An analysis of the model film pressure is given in figure 4, in which the simulation pressure is shown at $t = 120$ s for the 0.25 mL case. Using experimental film-thickness profiles as inputs, Hartland [7] predict corresponding film pressures via a numerical method: limits of variation in the derived film pressures for all experimental times later than $t = 90$ s are shown
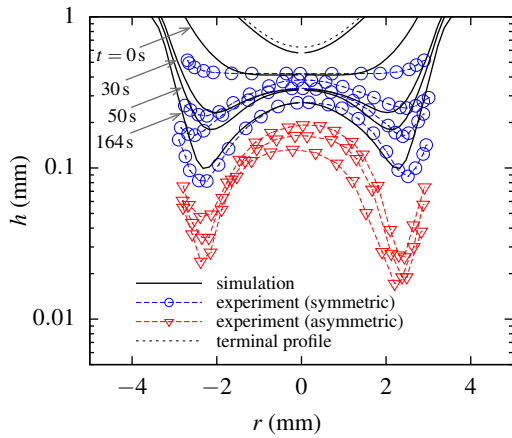
(a) 0.10 mL volume ($D_0 = 5.76$ mm)
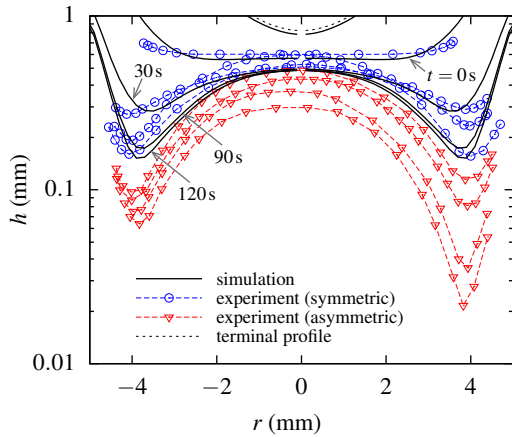
(b) 0.25 mL volume ($D_0 = 7.82$ mm)
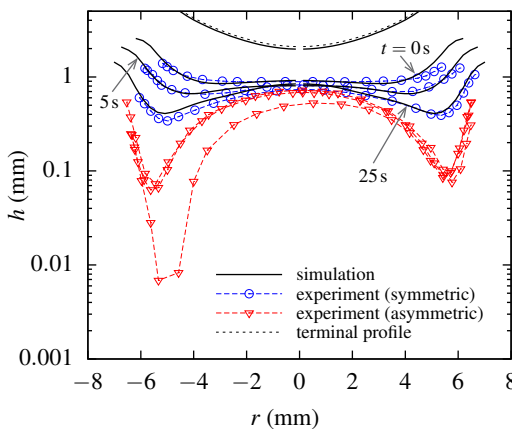
(c) 0.50 mL volume ($D_0 = 9.85$ mm)

Figure 2. Film-thickness profiles, h, at times corresponding to the experimental data of Hartland [6]. Simulation and experimental results are in good agreement until the onset of asymmetric film drainage. Note that reverse flow was observed in the 0.25 mL experiment, which cannot be captured with the present model implementation.
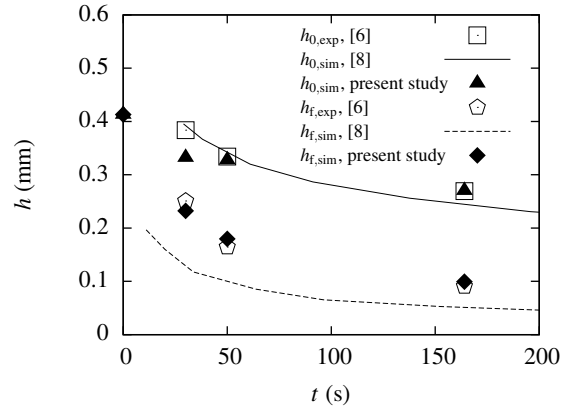
Figure 3. Film thickness at the centreline, h_0, and at the rim, h_f, for the 0.1 mL droplet case
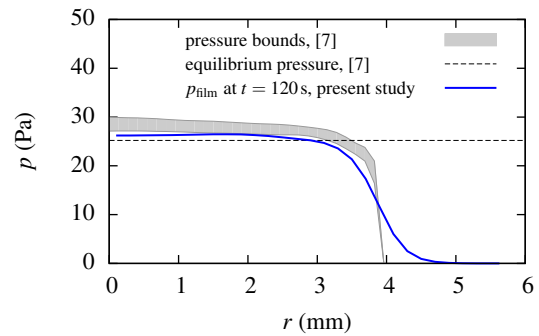
Figure 4. Simulation film pressure, p_{film}, and results of Hartland's [7] analysis for the 0.25 mL droplet case.

in figure 4. Also shown is the predicted film pressure for an equilibrium film of uniform, zero thickness [7]. The simulated film pressure at $t = 120$ s was found to be of the same magnitude as the equilibrium pressure, though slightly lower than the predicted pressure bounds of [7]. Note that the simulation film pressure trends smoothly to zero as the film thickness increases: the film pressure of [7] approaches zero at a predetermined film-radius, 3.96 mm in this case.

Droplet-scale Validation

Model and experiment droplet-scale cross sections for the 0.25 mL droplet are shown in figure 5. Note that the experimental image (figure 5a) shows the droplet silhouette, though the centre cross-section and inner dimple are still visible inside the droplet, as fluids of matched refractive index were used. The shape of the simulation cross-section (figure 5b) agrees well with that of the experiment, validating model performance at the droplet scale.
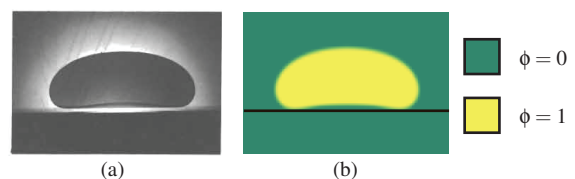
Figure 5. Droplet-scale cross section results for the 0.25 mL case at $t = 60$ s: (a) experiment [6] and (b) simulation. For illustration, the simulation results have been reflected in the rz-plane. Image ©1951–1971 AIChE, reproduced with permission.

Model Limitations

The current model implicitly assumes a fully mobile interface, hence the fluid shear stress and velocity are taken to be continuous across the two-phase boundary. We note that Hartland [6] concluded an immobile, zero-shear-stress interface was present at early experimental times, before transitioning to a mobile interface. Though not investigated in the present study, early-time influence of interface mobility could be explored via modification of the subgrid boundary condition, equation (12). Experimental complications also increased the uncertainty of the immobility finding [6]: reverse flow occurred into the film at early times (see figure 2b), decreasing the net drainage rate, while tilting of the droplet occurred at late times, increasing the drainage rate. Due to axisymmetric constraints, late-time tilting, and associated lateral motion, cannot be accounted for in the present model: the model is primarily applicable to smaller-diameter droplets, for which the tilting effect is less pronounced [6].

As per [6], electrostatic forces have been assumed to be negligible for the film thicknesses studied. For modelling of smaller film thickness with appreciable electrostatic forces, a disjoining-pressure treatment of the electric double layer terms should be included in equation (6).

In applying the CSF model [1], via equation 6, the droplet-scale mesh has been extended below the wall z-location (figure 1a). Viscous continuous phase interaction with the wall is not accurately accounted for, as fluid elements can pass directly through the wall, until reaching the outflow condition on the bottom of the domain. Accounting for these interactions by modifying conventional CFD wall boundary conditions to incorporate film-drainage equations, of a similar form to equation 14, is the focus of current research.

Conclusions

The buoyancy-driven collision between a free droplet and wall was modelled for a highly viscous liquid–liquid system. Droplet-scale dynamics were captured using an implicit level-set method with reinitialisation, while thin-film drainage dynamics were modelled using a coupled subgrid-scale volume-conservation equation.

Model predictions agree favourably with the experimental results of Hartland [6] for all droplet-volume cases considered. Model results were found to be more accurate, when tracking the barrier-rim thickness, than the numerical model of Hartland [8]. Droplet-scale cross-sectional profiles were shown to match those of the original experiment for the 0.25 mL volume case, while the radial pressure profile was found to asymptotically approach the predicted equilibrium profile of Hartland [7].

As per previous models [8], axial symmetry has been assumed meaning that the model cannot reproduce the tilting and non-uniform drainage behaviour that is exhibited at late times in the experimental data. Ongoing research focuses on addressing limitations of the model implementation including (i) extension of lubrication model from a linear to planar system of equations, enabling the simulation of glancing collisions and asymmetric film drainage, and (ii) accounting for wall-effects on the continuous-phase velocity field.

Acknowledgements

References

[1] Brackbill, J. U., Kothe, D. B. and Zemach, C., A continuum method for modeling surface tension, *J. Comput. Phys.*, **100**, 1992, 335–354.

[2] C. Ortiz-Dueãs and J. Kim and E. Longmire, Investigation of liquid–liquid drop coalescence using tomographic PIV, *Exp. Fluids*, **49**, 2010, 111–129.

[3] Chan, D. Y. C., Dagastine, R. R. and White, L. R., Forces between a rigid probe particle and a liquid interface. I. The repulsive case, *J. Colloid Interface Sci.*, **236**, 2001, 141–154.

[4] Eiswirth, R. T., Bart, H.-J., Ganguli, A. A. and Kenig, E. Y., Experimental and numerical investigation of binary coalescence: Liquid bridge building and internal flow fields, *Phys. Fluids*, **24**, 2012, 062108.

[5] Goodall, D. G., Gee, M. L. and Stevens, G. W., An imaging reflectometry study of the effect of electrolyte on the drainage and profile of an aqueous film between an oil droplet and a hydrophilic silica surface, *Langmuir*, **18**, 2002, 4729–4735.

[6] Hartland, S., The profile of the draining film beneath a liquid drop approaching a plane interface, *Chem. Eng. Prog. Symp. Ser.*, **91**, 1969, 82–89.

[7] Hartland, S., The pressure distribution in axisymmetric draining films, *J. Colloid Interface Sci.*, **35**, 1971, 227–237.

[8] Hartland, S., Yang, B. and Jeelani, S. A. K., Dimple formation in the thin film beneath a drop or bubble approaching a plane surface, *Chem. Eng. Sci.*, **49**, 1994, 1313–1322.

[9] Harvie, D. J. E., An implicit finite volume method for arbitrary transport equations, *ANZIAM J.*, **52**, 2012, C1126–C1145.

[10] Harvie, D. J. E. and Fletcher, D. F., A hydrodynamic and thermodynamic simulation of droplet impacts on hot surfaces, Part I: theoretical model, *Int. J. Heat Mass Transfer*, **44**, 2001, 2633–2642.

[11] Klaseboer, E., Chevaillier, J.-P., Maté, A., Masbernat, O. and Gourdon, C., Model and experiments of a drop impinging on an immersed wall, *Phys. Fluids*, **13**, 2001, 45–57.

[12] Manica, R., Hendrix, M. H. W., Gupta, R., Klaseboer, E., Ohl, C.-D. and Chan, D. Y. C., Effects of hydrodynamic film boundary conditions on bubble–wall impact, *Soft Matter*, **9**, 2013, 9755–9758.

[13] Mason, L. R., Stevens, G. W. and Harvie, D. J. E., Multi-scale volume of fluid modelling of droplet coalescence, in *Ninth International Conference on Computational Fluid Dynamics in the Minerals and Process Industries, Melbourne, Australia*, 2012.

[14] Quan, S., Dynamics and thin film drainage of a deformable droplet moving towards a solid wall with finite inertia, *RSC Advances*, **2**, 2012, 1927–1935.

[15] Sussman, M., Smereka, P. and Osher, S., A level set approach for computing solutions to incompressible two-phase flow, *J. Comput. Phys.*, **114**, 1994, 146–159.